

DOCUMENT CONTROL SHEET

	ORIGINATOR'S REF. NLR TP 96122 U		SECURITY CLASS. Unclassified												
ORIGINATOR National Aerospace Laboratory NLR, Amsterdam, The Netherlands															
TITLE Experimental validation of a lifting surface theory for rotor-stator interaction noise generation															
PRESENTED AT the 2nd AIAA/CEAS Aeroacoustics Conference, State College PA, May 6-8, 1996															
AUTHORS P. Sijtsma, E.R. Rademaker and J.B.H.M. Schulten		DATE 960220	pp ref 15 11												
DESCRIPTORS <table style="width: 100%; border: none;"> <tr> <td style="width: 50%;">Acoustic measurement</td> <td style="width: 50%;">Noise generators</td> </tr> <tr> <td>Engine noise</td> <td>Rotor blades (turbomachinery)</td> </tr> <tr> <td>Fan blades</td> <td>Stator blades</td> </tr> <tr> <td>Interactional aerodynamics</td> <td>Turbofans</td> </tr> <tr> <td>Nacelles</td> <td>Wall pressure</td> </tr> <tr> <td>Noise reduction</td> <td>Wind tunnel tests</td> </tr> </table>				Acoustic measurement	Noise generators	Engine noise	Rotor blades (turbomachinery)	Fan blades	Stator blades	Interactional aerodynamics	Turbofans	Nacelles	Wall pressure	Noise reduction	Wind tunnel tests
Acoustic measurement	Noise generators														
Engine noise	Rotor blades (turbomachinery)														
Fan blades	Stator blades														
Interactional aerodynamics	Turbofans														
Nacelles	Wall pressure														
Noise reduction	Wind tunnel tests														
ABSTRACT An important element in the NLR prediction model for rotor/stator interaction noise is the unsteady lifting surface theory for a rotating blade row. To validate this lifting surface theory a wind tunnel experiment has been carried out using a through-flow nacelle with a hub inside, a 16-bladed rotor and a 18-vanes stator. Sound was generated by stator vane interaction with the rotor viscous wakes and, due to the small gap between rotor and stator, also by stator vane interaction with the rotor blades displacement velocity and vice versa. Trip wires were attached to blades and vanes to simulate high Reynolds number flow. Unsteady pressures were measured on a stator vane, on a rotor blade and in the inlet. In this paper experiment and theory are briefly described and results from both are compared. For most of the measured cases, the agreement is good.															

NLR TECHNICAL PUBLICATION

TP 96122 U

EXPERIMENTAL VALIDATION OF A LIFTING SURFACE THEORY
FOR ROTOR-STATOR INTERACTION NOISE GENERATION

by

P. Sijtsma, E.R. Rademaker and J.B.H.M. Schulten

Paper presented at the 2nd AIAA/CEAS Aeroacoustics Conference, State College PA, May 6-8, 1996.

This investigation has been carried out under a contract awarded by the Netherlands Agency for Aerospace Programs, contract number 01402 N.

Division : Fluid Dynamics

Prepared : PS/ *BERR* / *JBHM*

Approved : HHB/ *SB*

Completed : 960220

Order number: 101.922

Typ. : MM



Contents

Nomenclature	5
I. Introduction	5
II. Rotor-stator interaction	6
III. Theoretical Model	7
IV. Experimental model	8
V. Validation	9
VI. Conclusions	15
References	15

1 Table
23 Figures

(15 pages in total)



This page is intentionally left blank.



EXPERIMENTAL VALIDATION OF A LIFTING SURFACE THEORY FOR ROTOR-STATOR INTERACTION NOISE GENERATION

Pieter Sijtsma*, Edward R. Rademaker*, and Johan B.H.M. Schulten†
National Aerospace Laboratory NLR, 8300 AD Emmeloord, The Netherlands

An important element in the NLR prediction model for rotor-stator interaction noise is the unsteady lifting surface theory for a rotating blade row. To validate this lifting surface theory a wind tunnel experiment has been carried out using a through-flow nacelle with a hub inside, a 16-bladed rotor and a 18-vanes stator. Sound was generated by stator vane interaction with the rotor viscous wakes and, due to the small gap between rotor and stator, also by stator vane interaction with the rotor blades displacement velocity and vice versa. Trip wires were attached to blades and vanes to simulate high Reynolds number flow. Unsteady pressures were measured on a stator vane, on a rotor blade and in the inlet. In this paper experiment and theory are briefly described and results from both are compared. For most of the measured cases, the agreement is good.

Nomenclature

B	= number of rotor blades
C_p	= pressure coefficient
h	= hub radius
i	= imaginary unit
J_m	= m -th order Bessel function of the first kind
k	= circumferential mode number (incident field)
M	= Mach number of axial flow
m	= circumferential mode number (resulting field)
p	= pressure disturbance
RPM	= revolutions per minute
RPM_0	= nominal RPM (Eq. (17))
r	= radial coordinate
$U_{m\mu}$	= radial eigenfunction
V	= number of stator vanes
v	= disturbance velocity
x	= axial coordinate
Y_m	= m -th order Bessel function of the second kind
α	= axial wave number
β	= $(1-M^2)^{1/2}$
ε	= eigenvalue
θ	= circumferential coordinate
μ	= radial mode number
Ω	= circumferential tip-Mach number
ω	= frequency (dimensionless)
ω_k	= frequency of incident field
ω_l	= frequency in blade fixed frame
ω_m	= frequency of resulting field

I. Introduction

In the development of turbofan engines for civil aircraft, there is a trend to higher and higher bypass ratios. New engines have lower fan speeds and are quieter than the older models. A low fan speed is important, because an isolated fan does not produce sound when it operates at subsonic relative (helical) tip speed. Then, the interaction of the fan (rotor) with the downstream stator is the most important noise generating mechanism.

Rotor-stator interaction is a complicated process. Both rotor and stator generate flow distortions, thus inducing unsteady loading on each other. Consequently, both rotor and stator act as sound sources. Sound waves are generated at the rotor blade-passing frequency (BPF) and its higher harmonics. Their circumferential mode numbers are linear combinations of the number of rotor blades and the number of stator vanes¹. Usually, these numbers are chosen such that the first harmonic is cut-off.

In order to describe the several aspects of rotor-stator interaction and to predict the resulting noise, a theoretical model was developed, based on lifting surface theory². In this model a uniform main flow is assumed, compared to which the distortions caused by rotor and stator are small. Additionally, computer programs were written to quantify the noise sources. The theory can be used to optimize the shielding effect of a rotor³.

Part of the theory was validated in 1987 by an experiment in the NLR Low Speed Wind Tunnel by Zandbergen^{4,5}. A row of 18 stator vanes was installed in a through-flow nacelle and a set of 16 rotating rods was used to generate viscous wakes. The unsteady wake velocities were measured and, with this measured incident field, the unsteady stator loading was numerically predicted. On an instrumented stator vane, the unsteady pressure was measured and compared with numerical results. Although the velocity distortions were rather high (up to 20 percent of the main velocity), the experimental and numerical results agreed very well⁶.

Supported by the Netherlands Agency for Aerospace Programs NIVR, Contract 01402N.

Copyright © 1996 by the American Institute of Aeronautics and Astronautics, Inc. All rights reserved.

*Research Engineer, Aeroacoustics Department.

†Senior Research Engineer, Aeroacoustics Department, Senior Member AIAA.

In 1995 an experiment with the same fan model was carried out, but this time with the rods replaced by an actual, unloaded rotor. Trip wires were attached to both sides of each rotor blade and each stator vane, in order to fix the transition from laminar to turbulent boundary layer flow. One of the rotor blades was instrumented at midspan in order to measure the local unsteady loading. Further, the resulting sound in the intake was measured using an annular array of transducers, mounted in the duct wall.

The axial gap between rotor and stator was small and therefore, the primary noise sources were not only the viscous wakes from the rotor blades, but also the displacement velocity of rotor blades and stator vanes.

The goal of this new experiment was to validate the lifting surface theory for a rotating blade row, so that the theory could be used with some confidence to include the effect of rotor shielding. In this paper the comparison of experimental and theoretical results is discussed.

This paper is organised as follows. In Sec. II the physics of rotor-stator interaction noise generation are reviewed. Sec. III briefly outlines the theoretical modelling and Sec. IV gives a description of the experiment. Sec. V describes the validation and the conclusions are stated in Sec. VI.

II. Rotor-stator interaction

As in Ref. 2, we consider an annular flow duct with a uniform, subsonic main flow of Mach number M . The flow is assumed to be inviscid and isentropic. Noise is induced by flow distortions, which are supposed to be small.

In this section we discuss the kinds of flow distortions that can be distinguished, it is briefly discussed what happens when a rotating blade row experiences an unsteady flow distortion and the features of rotor-stator interaction noise are reviewed.

The physical properties that we consider are made dimensionless using the duct radius, the ambient density and the ambient speed of sound. Cylindrical coordinates (x, r, θ) are defined in the duct.

Flow distortions

Under the above mentioned restrictions, the governing equations for the dimensionless disturbance pressure p and velocity \mathbf{v} read

$$\frac{Dp}{Dt} + \nabla \cdot \mathbf{v} = 0, \quad (1)$$

$$\frac{D\mathbf{v}}{Dt} + \nabla p = 0, \quad (2)$$

where

$$\frac{D}{Dt} = \frac{\partial}{\partial t} + M \frac{\partial}{\partial x}. \quad (3)$$

Two classes of solutions can be distinguished.

The first class consists of solutions with $p = 0$. Possible solutions for \mathbf{v} can be written as:

$$\mathbf{v} = \nabla \times U(t - \frac{x}{M}, \theta, r), \quad (4)$$

where $\nabla \times$ is the curl operator. For a single dimensionless frequency ω and circumferential mode number m , Eq. (4) reduces to:

$$\mathbf{v} = \nabla \times \left\{ e^{i[\omega(t - \frac{x}{M}) + m\theta]} U(r) \right\}, \quad (5)$$

where i is the imaginary unit. These solutions are called vortical waves. Vortical waves always are convected downstream from the source.

The second class consists of solutions with non-zero p , governed by the convective Helmholtz equation:

$$\frac{D^2 p}{Dt^2} - \nabla^2 p = 0. \quad (6)$$

Solutions (modes) with specified ω and m have the form:

$$p(x, r, \theta, t) = A e^{i(\omega t - \alpha x + m\theta)} U_{m\mu}(r), \quad (7)$$

where A is the modal amplitude and $U_{m\mu}$ is a radial eigenfunction, satisfying the hard wall boundary condition at $r = h$ (hub) and $r = l$ (shroud). The axial wave numbers α follow from the dispersion relation:

$$\alpha = \frac{1}{\beta^2} \left(M\omega \pm (\omega^2 - \beta^2 \varepsilon^2)^{1/2} \right). \quad (8)$$

Herein $\beta^2 = 1 - M^2$ and ε is a solution of:

$$J'_m(\varepsilon) Y'_m(\varepsilon h) - Y'_m(\varepsilon) J'_m(\varepsilon h) = 0, \quad (9)$$

where J_m and Y_m are m -th order Bessel function of the first and the second kind, respectively. The unsteady velocity \mathbf{v} , associated with Eq. (7), follows from Eq. (2) and has the form:

$$\mathbf{v} = \frac{-A}{i(\omega + M\alpha)} \begin{pmatrix} i\alpha \\ \partial/\partial r \\ im/r \end{pmatrix} e^{i(\omega t + \alpha x + m\theta)} U_{m\mu}(r). \quad (10)$$

These solutions are acoustic waves. Acoustic waves propagate both upstream and downstream from the source.

Within the acoustic waves, we can identify propagating or cut-on modes and non-propagating or cut-off modes. Cut-on modes are modes for which α is real ($\omega^2 \geq \beta^2 \varepsilon^2$), cut-off modes are modes for which α has a non-zero imaginary part ($\omega^2 < \beta^2 \varepsilon^2$). Resonance occurs when $\omega^2 = \beta^2 \varepsilon^2$.

The interaction mechanism

Suppose that the main flow is disturbed by an unsteady vortical or acoustic wave of frequency ω_k and circumferential mode number k :

$$w(x, r, \theta, t) = w_k(x, r) e^{i(\omega_k t + k\theta)} \quad (11)$$

Then, the blades of a blade row which rotates with tip-Mach number Ω experience a flow distortion of frequency

$$\omega_l = \omega_k + k\Omega. \quad (12)$$

As a reaction, unsteady pressure jumps are induced across the blade surfaces, with the same frequency. Consequently, the blade row acts as a source for a sequence of acoustic waves with frequencies

$$\omega_m = \omega_k + nB\Omega, \quad n = \dots, -2, -1, 0, 1, 2, \dots, \quad (13)$$

where B is the number of blades. The corresponding circumferential mode numbers are

$$m = k + nB. \quad (14)$$

Interaction noise

Consider a rotor with B blades, rotating with tangential tip-Mach number Ω , and a downstream stator with vane number V . Flow distortions which induce rotor-stator interaction noise are:

- The rotor bound potential field caused by steady loading of the rotor blades (acoustic modes).
- The stator bound potential field caused by steady loading of the stator vanes (non-propagating "acoustic modes" of zero frequency).
- The rotor bound potential field caused by displacement of the rotor blades (acoustic modes).
- The stator bound potential field caused by displacement of the stator vanes (non-propagating "acoustic modes" of zero frequency).
- The downstream convected vortical wakes caused by steady loading of the rotor blades.
- The downstream convected viscous wakes which are caused by the boundary layer development at the rotor blade surfaces.

The distortions caused by displacement (c.,d.) quickly diminish for increasing rotor-stator gap. In a full size turbofan they are negligible. Further, the acoustic distortions a. and b. are usually weak compared to the convective distortions e. and f.

The viscous wakes (f.) do not fall within the inviscid approach, but a well-developed turbulent wake can be modeled by a shear layer⁷, in other words, by a vortical wake.

The rotor-induced distortions (a.,c.,e.,f.) have frequencies $n_1 B \Omega$ and mode numbers $-n_1 B$. By the interaction at the

stator, acoustic waves are produced with frequencies $n_1 B \Omega$ and mode numbers $-n_1 B - n_2 V$. These waves impinge on the rotor, which then produces acoustic waves with frequencies $(n_1 + n_3) B \Omega$ and mode numbers $-(n_1 + n_3) B - n_2 V$. So, each harmonic (n_1) of the unsteady loading on the stator vanes contributes to each harmonic ($n_1 + n_3$) in front of the rotor.

Furthermore, the stator-induced distortions (b.,d.) have zero frequency and mode numbers $-n_2 V$. By the interaction at the rotor, acoustic waves are produced with frequencies $n_3 B \Omega$ and mode numbers $-n_3 B - n_2 V$.

Acoustic waves, generated at the rotor, impinge on the stator, where new acoustic waves are formed. These diffracted waves interact with the rotor, where again new acoustic waves are formed, and so on. The process of interaction continually repeats itself. However, the newly created waves become weaker at each "iteration step".

So, to obtain the sound in front of the rotor, many components have to be summed:

- Sound generated at the stator by the interaction with rotor induced flow distortions.
- Sound generated at the rotor by the interaction with stator induced flow distortions.
- Sound generated at the rotor by the interaction with acoustic waves from the stator (rotor diffraction).
- Sound generated by multiple diffraction on stator and rotor.

III. Theoretical model

In this paper, the lifting surface theory described in Ref. 2 is to be validated. In this theory the flow is inviscid and isentropic. A uniform subsonic main flow is assumed, on which small distortions are superposed governed by Eqs. (1) and (2). As described in Sec. II, vortical and acoustic waves can be distinguished.

The blades of a blade row (rotor or stator) are modelled by lifting surfaces, i.e., infinitely thin reference surfaces across which steady and unsteady pressure discontinuities are allowed. The blade thickness is modelled by velocity monopoles, located at the reference surfaces. This lifting surface model is consistent with the linearized theory. Linearized theory fails when the blades are too heavily loaded or too thick.

Most difficult part of the theory is to obtain the pressure jump across the reference surface, given an incident field. The pressure jump or loading Δp satisfies a Fredholm integral equation of the first kind, symbolically written:

$$\int K(z, \zeta) \Delta p(\zeta) d\zeta = f(z). \quad (15)$$

When unsteady loading is considered, the right hand side f follows from the incident field. For the steady loading problem, f also depends on angle of incidence, blade camber and blade thickness. The kernel K only depends on the characteristics of the blade planform.

The unknown loading Δp is solved from Eq. (15) by expressing it in a series of suitably chosen basis functions and

by applying Galerkin projection. Then the unknown pressure coefficients can be solved from a linear system of equations:

$$LP=R, \quad (16)$$

where L is a matrix of influence coefficients, P is a vector of pressure coefficients and R is a vector which follows from the incident field.

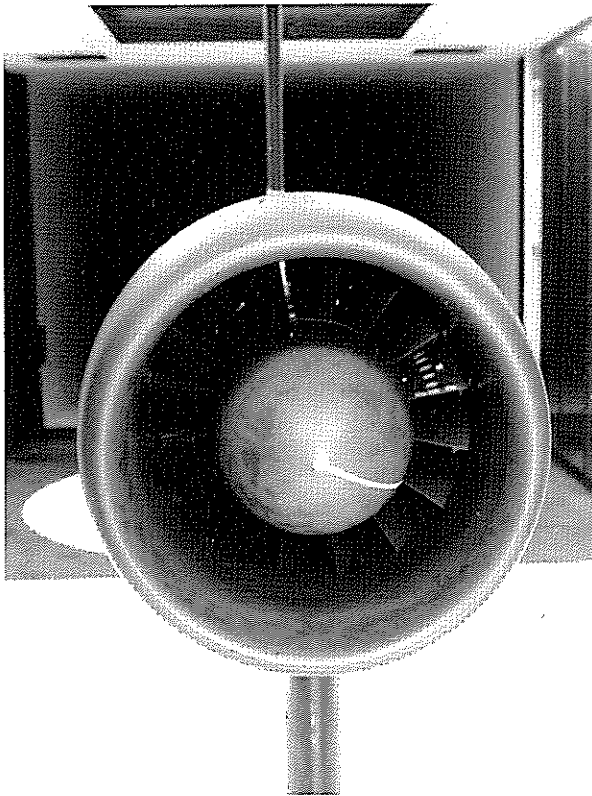


Fig. 1 Fan noise model.

Based on this lifting surface theory, computer programs were written. The use of these programs is restricted to unswept blades: the leading and the trailing edge are assumed to be in planes perpendicular to the axis. In other words, the x -coordinates of the edges do not vary in spanwise direction. With this geometrical restriction, separation of variables can be applied and the computational effort is much less than it would be for more general blade shapes. For swept blades, an alternative approach is given in Ref. 8.

IV. Experimental model

Set up

The experiment was carried out with an axisymmetric nacelle, placed in the NLR Low Speed Wind Tunnel (Fig. 1). This nacelle consists of a duct with a hub inside, connected by struts at the rear and a row of equidistant stator vanes, more upstream (see Fig. 2). Upstream of the stator, a rotor is mounted, driven by an air motor inside the hub. The diameter

of the flow tube is 400 mm, the diameter of the hub is 240 mm, the gap between rotor and stator is 15 mm.

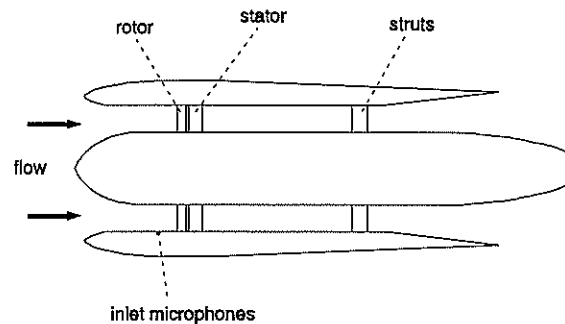


Fig. 2 Schematic drawing of experimental model.

The stator consists of 18 unleaned and unswept vanes aligned with the uniform flow. Their chordwise sections are uncambered NACA 0010-35 wing sections, which have a thickness of 10 percent. The chord length, which is constant along the span, is 50 mm.

Along a chordwise section of one of the stator vanes, 20 miniature transducers are mounted, symmetrically at lower and upper side. This particular vane is movable in radial direction, such that measurements can be done at several spanwise positions. Measurements were carried out at three positions: 30 percent annular span (from the hub), 53 percent span and 76 percent span.

The rotor consists of 16 unleaned and unswept blades. The stagger angles are adjusted such that the incident relative flow angle is zero when the rotor rotates with 6650 revolutions per minute (RPM) and the axial flow is 85 m/s. The blades have constant axial chord length of 40 mm, hence the actual chord length varies in spanwise (radial) direction. The blade section at the hub is a NACA 0010-35 section, at other radii modified NACA 0010-35 sections are used. The relative thickness of these modified sections is reduced such that the absolute maximum thickness is constant.

Also one of the rotor blades is equipped with transducers, 6 at each side of the midspan section. Since a rotor blade is not movable without violating the geometry, only at this one radius measurements can be carried out.

Furthermore, an annular array of 22 equidistant transducers was installed at the inner wall of the duct, 80 mm upstream from the rotor, to measure the unsteady wall pressures of circumferential modes.

For convenience, some dimensionless coordinates are listed in Table 1.

Trip wires

During the tests, the axial Mach number was varied from 0.10 to 0.23. As a result, the Reynolds number of the flow along the blades had values between 10^5 and 10^6 , a region in which transition from laminar to turbulent boundary layer flow is very sensitive to the Reynolds number. Therefore, it could be possible that the location of the transition varied with time and the motion of the transition points would affect

Table 1: Dimensionless coordinates of experimental set up

nacelle	tip radius	$r = 1$
	hub radius	$h = 0.6$
	intake transducers	$x = 0$
rotor	blade number	$B = 16$
	leading edge	$x = 0.400$
	trailing edge	$x = 0.600$
	transducers	$r = 0.800$
stator	vane number	$V = 18$
	leading edge	$x = 0.675$
	trailing edge	$x = 0.925$
	transducers	$r = 0.720$
		$r = 0.813$ $r = 0.905$

the generation of sound in an unpredictable manner. To suppress this undesirable effect, which does not occur at the high Reynolds numbers in a full size turbofan, trip wires were attached at midchord, to both sides of rotor blades and stator vanes.

At the end of the measurements the trip wires on the rotor blades were removed and new measurements were carried out to investigate the difference. At the stator only one radial microphone position was then considered, namely $r = 0.720$.

Conditions

Measurements with the tripped and the untripped rotor were carried out at seven different rotor RPM's. The nominal RPM varied from 3240 to 6425. Nominal RPM (RPM_0) is defined as:

$$RPM_0 = RPM \cdot \sqrt{T_0/T}, \quad (17)$$

where T is the actual temperature and T_0 is the standard temperature (288.16 K). Hence, the tip-Mach number Ω of the rotor was chosen in advance, but the actual RPM depended on the temperature. The Mach numbers of the main flow in the duct were adjusted such that the steady loading of the rotor is as small as possible.

With the present setup and conditions, rotor and stator have no steady loading and sound will be generated by the viscous wakes from the rotor and by the displacement velocity of the rotor blades and the stator vanes. It is noted that the rotor blades and the stator vanes are much thicker and the rotor-

stator gap is much smaller than in an actual turbofan engine, where the influence of displacement velocity is negligible.

V. Validation

The aim of the experiment was to validate the lifting surface theory for a rotating blade row (the rotor), using a known incident acoustic field. As mentioned in the introduction, the unsteady lifting surface theory was already validated for a stator in 1987^{4,5}.

The incident field on the rotor is induced by the unsteady loading and the displacement of the stator vanes. The displacement part of the incident field must be calculated, but for the loading part we could use the measurements. We will use, however, calculated stator loading to be assured that the phases of the different contributions to the incident field are in the correct proportion. Due to the small gap between rotor and stator, some adjustment to the calculated stator loading will be needed, as will be described in the following.

Stator

Unsteady stator loading is caused by several types of interaction: interaction with steady and unsteady loading of the rotor blades (acoustic modes as well as vortices), interaction with the rotor displacement field and interaction with viscous wakes. In the present experiment only the latter two give significant contributions.

Drag coefficients

In the viscous wake model, i.e., Schlichting's turbulent wake model⁷, the drag coefficients of the rotor blade sections are required as input. For high Reynolds numbers ($Re \geq 3 \cdot 10^6$) the drag coefficient of a smooth NACA 0010-35 section is known from Ref. 9. However, in the experiment the Reynolds numbers are much lower, between 10^5 and 10^6 . Moreover, only at the hub a genuine NACA 0010-35 section is used for the rotor blade section. At other radial positions modified versions of this section are used (see Sec. IV). Furthermore, attached trip wires will affect the drag as well.

To obtain the required drag coefficients, measurements were performed of wake velocities behind wing sections. Two constant chord models were manufactured especially for this purpose: a thick model, with cross section identical to the stator vane sections and the rotor hub sections blades (NACA 0010-35), and a thin model, with cross section identical to the rotor tip sections. The wake measurements were carried out with and without trip wires. The Reynolds number range was the same as in the fan experiment.

The measured drag coefficients, together with least squares fits, are plotted in Figures 3 and 4 as a function of the Reynolds number. The measurements show that, for not too low Reynolds number, tripping the wings causes the drag to increase significantly, up to a factor 2.

The measurements behind the thick model (Fig. 3) demonstrate that the drag of the untripped model is very sensitive to the Reynolds number, in contrast with the drag of the tripped model. This illustrates the benefit of the trip wires, in particular at lower Reynolds numbers occurring at the stator vanes and at the hub sections of the rotor blades.

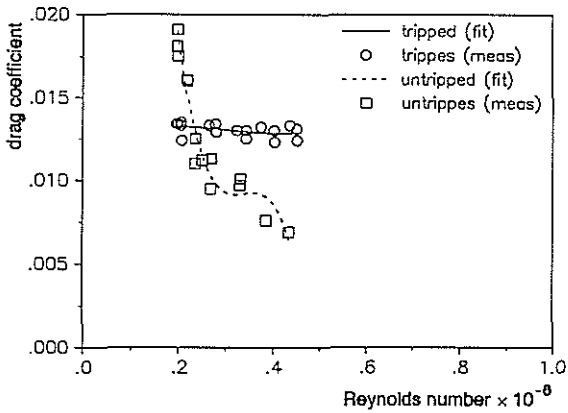


Fig. 3 Drag coefficients of rotor hub section (thick model).

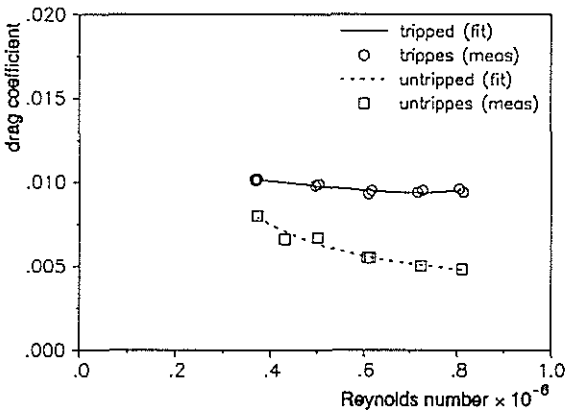


Fig. 4 Drag coefficients of rotor tip section (thin model).

As input for the theoretical model the least squares fits (Figs. 3, 4) of the drag coefficients were used for the sections at the hub and the tip. For sections in between, the drag coefficient has been assumed to vary linearly with the radial coordinate.

Rotor blades displacement

A complication which arises when calculating the unsteady stator loading is caused by the thickness of the rotor blades. The rotor blade sections have a maximum thickness of 10 percent, considerably thicker than commonly used in turbofans. This blade thickness was needed to accommodate the pressure transducers. However, it is too thick to carelessly apply linearized theory for calculating the displacement velocity. Due to the boundary layer, the effective thickness is

even more than 10 percent. Linearized theory tends to underpredict the actual distortion for such thick blades. (This can be verified by sample calculations of two-dimensional potential flow around Joukowski airfoils, see Ref. 10.)

In the experiment the gap between rotor and stator is much smaller than usual and, as a result, the interaction with the rotor displacement field plays an important role in the first harmonic stator loading. For higher harmonics the influence of rotor displacement rapidly vanishes.

In Figures 5, 6 and 7 results are shown for the first three harmonics at $r = 0.813$ of the unsteady stator loading for the case of 5550 RPM₀. The computed as well as the measured moduli of the pressure jumps are plotted. Moreover, the (computed) contributions of rotor displacement and viscous wakes are shown. It is noted that the two contributions are in counter-phase in the first harmonic and in phase in the second harmonic. In the third harmonic the influence of rotor thickness is negligible.

The computed results in the first harmonic (Fig. 5) are significantly lower than the measured results. The reason for this discrepancy is probably that the theory underpredicts the contribution of the rotor displacement thickness. If this contribution is multiplied with a "nonlinearity" factor 1.4, a much better agreement is found (see Fig. 8). For higher harmonics (Figs. 6, 7) such a multiplication does not affect the good agreement.

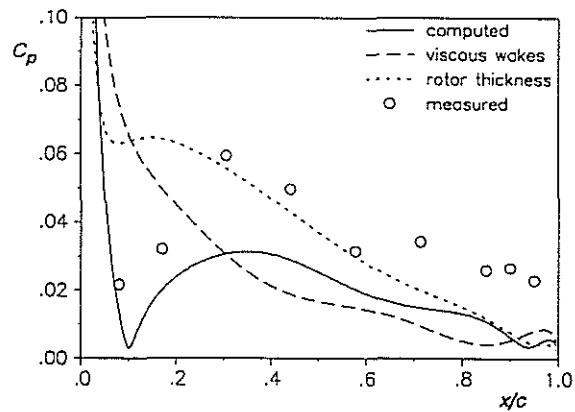


Fig. 5 Stator unsteady pressure, 5550 RPM₀, modulus of pressure jump at $r = 0.8125$, 1st harmonic.

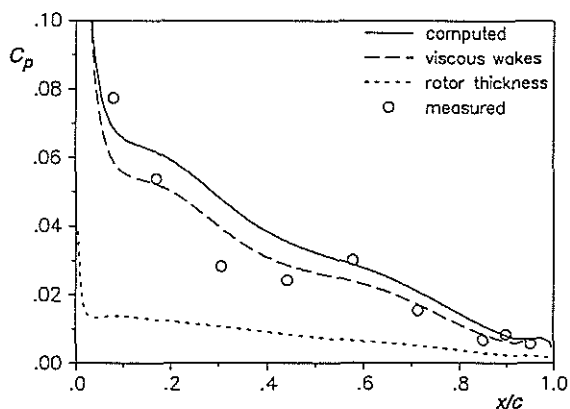


Fig. 6 Same conditions as Figure 5, 2nd harmonic.

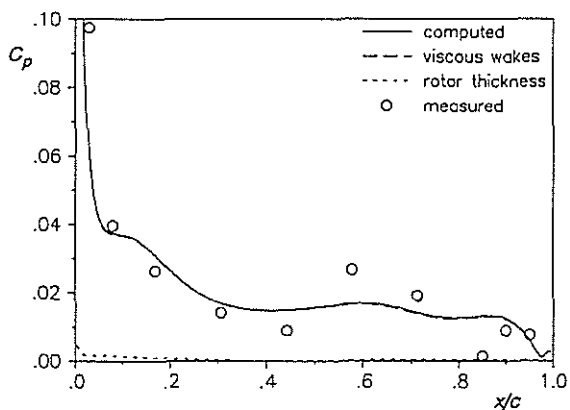


Fig. 7 Same conditions as Figure 5, 3rd harmonic.

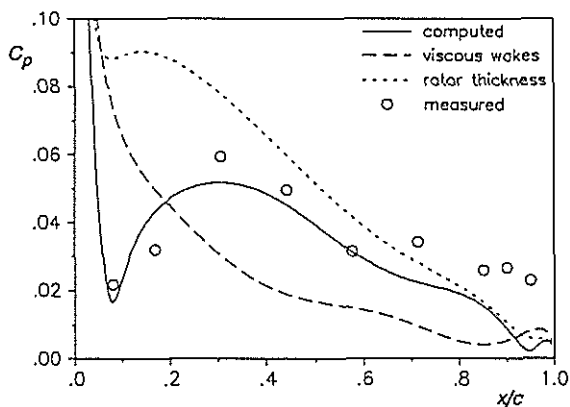


Fig. 8 Same conditions as Figure 5, calculated with 'nonlinear' correction.

The same procedure, i.e., multiplying the thickness contribution in the stator first harmonic with 1.4, is followed for other RPM₀'s and with the untripped rotor. In each case and for each harmonic good agreement is found. The thus obtained unsteady stator pressures are used as input for the unsteady rotor calculations.

Rotor

The unsteady pressure on the rotor blades is induced by incident acoustic modes, radiating from the stator, with frequencies $\omega_k = n_1 \times 16\Omega$ and mode numbers $k = -n_1 \times 16 - n_2 \times 18$ (see Sec. II). The induced unsteady rotor blade loading consists of frequencies:

$$\omega_l = -n_1 \times 16\Omega - (-n_1 \times 16 - n_2 \times 18)\Omega = n_2 \times 18\Omega \quad (18)$$

(see Eq. (12)). In other words, the unsteady rotor pressure is periodic with the stator vane passing frequency. It follows that each harmonic (n_1) on the stator contributes to each harmonic (n_2) on the rotor.

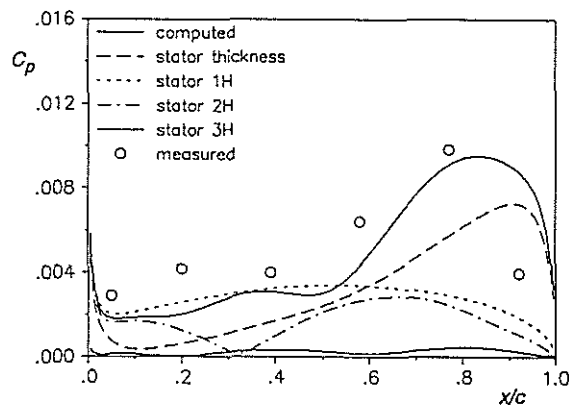


Fig. 9 Rotor unsteady pressure, 5550 RPM₀, modulus of pressure jump at midspan, 1st harmonic.

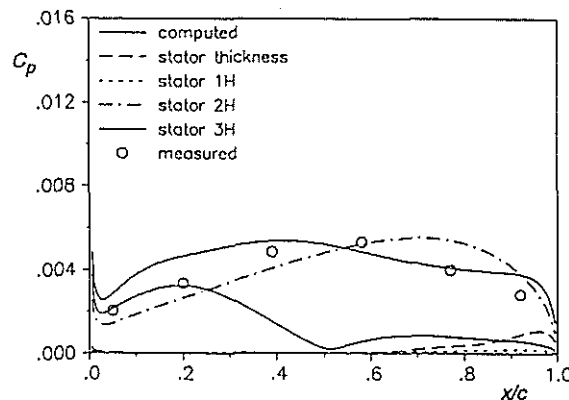


Fig. 10 Same conditions as Figure 9, 2nd harmonic.

For the rotor first and second harmonic ($n_2 = 1,2$), which are the cases considered in the validation, it appears that only the stator first, second and third harmonic ($n_1 = 1,2,3$) contribute significantly. Higher harmonics ($n_1 > 3$) and steady loading ($n_1 = 0$) on the stator have negligible influence.

An other contribution to the unsteady loading of the rotor blades is the (steady) displacement velocity induced by the thickness of the stator vanes. This field can be decomposed in "acoustic" modes of zero frequency, $\omega_k = 0$, and mode numbers $k = -n_2 \times 18$. Again, the corresponding frequencies at the rotor blades are given by Eq. (18).

In Fig. 9 the computed and measured first harmonic unsteady rotor loading at 5550 RPM₀ is plotted. Also the several components which contribute to the total loading are plotted. In Fig. 10 similar results are plotted for the second harmonic. It is seen that, though it is a complicated process to compute the total loading, in which several contributions are of the same order of magnitude, the agreement with the measurements is good.

In Figures 11 to 17 the measured and computed, first and second harmonic of the rotor loading are plotted, without showing the several components by which it is built up. This is done for the entire range of RPM₀'s (from 3240 to 6425).

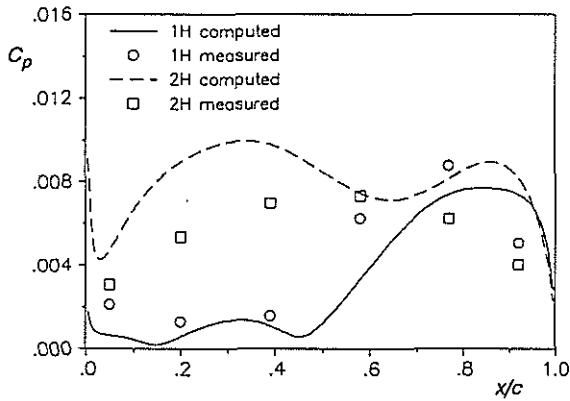


Fig. 11 Rotor unsteady pressure, 3240 RPM₀, modulus of pressure jump at midspan, 1st and 2nd harmonic.

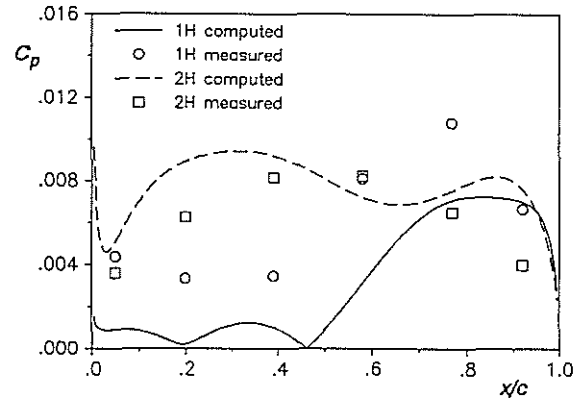


Fig. 12 Rotor unsteady pressure, 3865 RPM₀, modulus of pressure jump at midspan, 1st and 2nd harmonic.

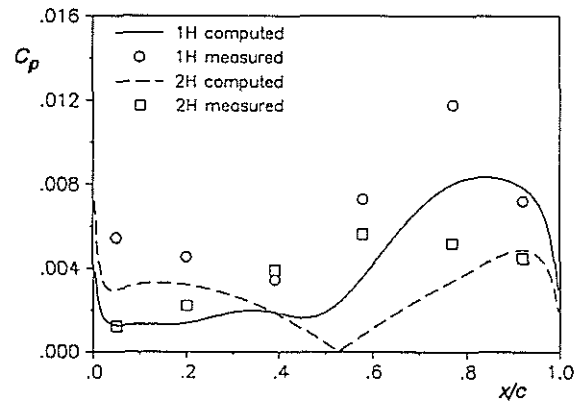


Fig. 13 Rotor unsteady pressure, 4565 RPM₀, modulus of pressure jump at midspan, 1st and 2nd harmonic.

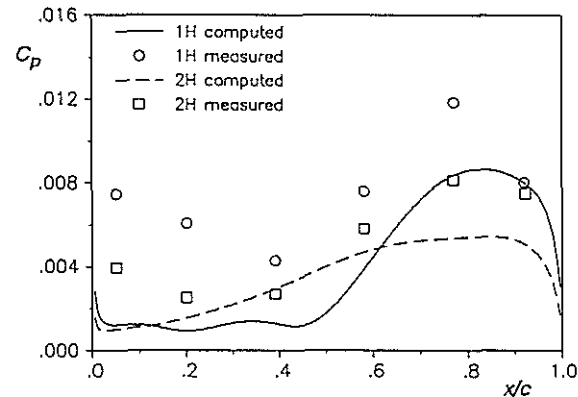


Fig. 14 Rotor unsteady pressure, 4750 RPM₀, modulus of pressure jump at midspan, 1st and 2nd harmonic.

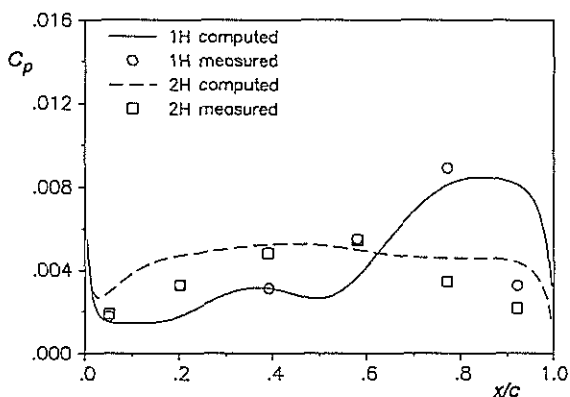


Fig. 15 Rotor unsteady pressure, 5440 RPM_0 , modulus of pressure jump at midspan, 1st and 2nd harmonic.

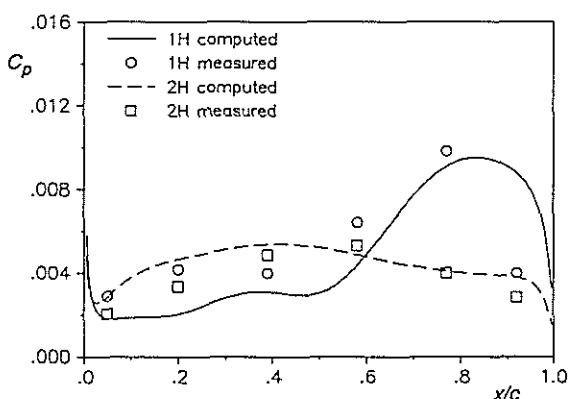


Fig. 16 Rotor unsteady pressure, 5550 RPM_0 , modulus of pressure jump at midspan, 1st and 2nd harmonic.

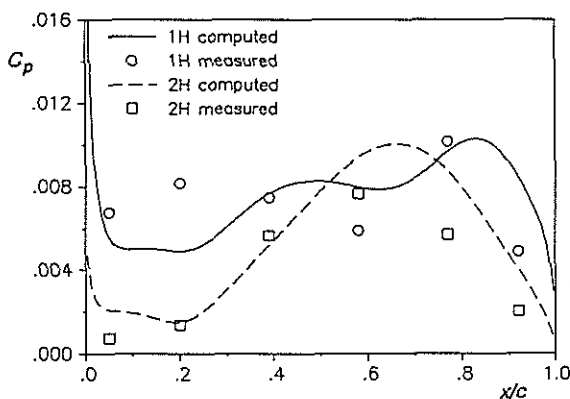


Fig. 17 Rotor unsteady pressure, 6425 RPM_0 , modulus of pressure jump at midspan, 1st and 2nd harmonic.

It is seen that the agreement between theory and experiment gets better as the RPM_0 increases. Probably this is due to a decrease of inlet reflections, which are not included in the present calculations.

An estimation for the inlet reflections can be obtained using Wiener-Hopf theory for a sharp-edged semi-infinitely long duct with a two-sided infinitely long hub¹¹. In the considered RPM_0 range only the first radial mode ($\mu = 1$) of the first harmonic (with $k = 2$) is cut-on. Inlet reflection coefficients are plotted in Fig. 18. This explains, at least for the first harmonic, why the agreement between theory and experiment gets better as the RPM_0 increases.

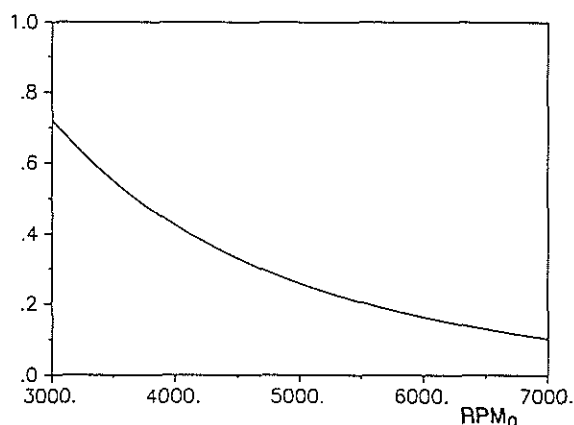


Fig. 18 Reflection coefficient of the first harmonic acoustic pressure, $k = 2$.

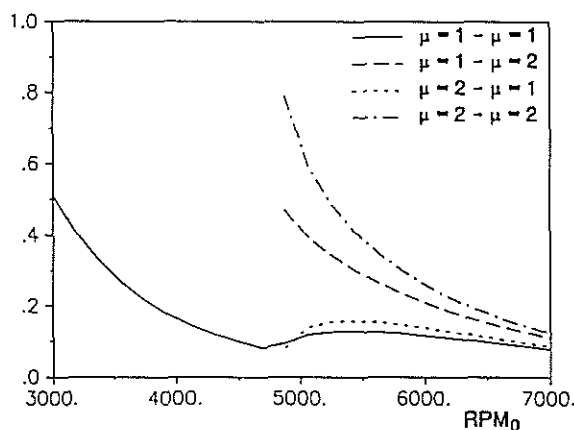


Fig. 19 Reflection coefficients of the second harmonic acoustic pressure, $k = 4$.

For the second harmonic (with $k = 4$) the situation is more complicated, since starting from 4800 RPM_0 the second radial mode ($\mu = 2$) is also cut-on. In that case at the inlet plane not only single-mode reflections occur, but also scattering from one mode to the other, i.e., from $\mu = 1$ to $\mu = 2$ and vice versa. The reflection coefficients are plotted in Fig. 19. It



must be noted, however, that for 5440 and 5550 RPM₀, the agreement between theory and measurement is still good (Figs. 15, 16), despite the strong reflections that can be expected in those cases.

Inlet

Three source mechanisms contributing to the resulting acoustic pressure in the duct inlet can be distinguished. First, from the stator acoustic modes emanate with frequencies $\omega_k = n_1 \times 16\Omega$ and mode numbers $k = -n_1 \times 16 - n_2 \times 18$. Secondly, by interaction with the rotor, modes arise with frequencies $\omega_k = (n_1 + n_3) \times 16\Omega$ and mode numbers $k = -(n_1 + n_3) \times 16 - n_2 \times 18$. The third contribution is the interaction of the rotor with the stator induced steady displacement velocity, yielding an acoustic field with frequencies $\omega_k = n_3 \times 16\Omega$ and mode numbers $k = -n_3 \times 16 - n_2 \times 18$.

In each case acoustic modes appear with frequencies $\omega_k = n \times 16\Omega$ and mode numbers $k = -n \times 16 - n_2 \times 18$, such in accordance with the theory of Ref. 1. For the first harmonic ($n = 1$) the only radial cut-on mode in the considered frequency range is the mode with the lowest circumferential mode number, that is $k = 2$, obtained with $n_2 = -1$. For the second harmonic ($n = 2$) the only cut-on mode is $k = 4$, obtained with $n_2 = -2$.

To illustrate the importance of the several sources, we consider again the case of 5550 RPM₀. The pressure amplitude of the first harmonic (with $k = 2$), computed at the inlet wall, is a summation of several contributions with the following amplitudes:

Direct radiation from the stator:	11.6 Pa
Interaction of rotor with stator thickness:	10.8 Pa
Interaction of rotor with stator first harmonic:	14.7 Pa
Interaction of rotor with stator second harmonic:	7.0 Pa
Interaction of rotor with stator third harmonic:	0.6 Pa

Summation of these contributions, each with its own phase, yields a pressure amplitude of 22.6 Pa. The measured counterpart in this case was 21.7 Pa. So, the computed and the measured inlet pressures amplitudes are remarkably close to each other. On a dB-scale the difference is only 0.35 dB, which is within the accuracy of the measurements.

In Fig. 20 the Sound Pressure Levels (SPL) are plotted of the computed and measured first harmonic ($k = 2$) inlet wall pressures. The agreement between computed and measured results gets better as the RPM₀ increases. The (small) disagreements at the lowest RPM₀'s can be explained by the inlet reflections (Fig. 18).

In Fig. 21 similar results are plotted, but now for the untripped rotor. For lower RPM₀'s the differences between experiment and theory is larger than with the tripped rotor. In some cases the difference is too large to be explained by inlet reflections. A possible explanation is that, due to the absence of trip wires, the transition points on the rotor blades vary with time and act as new displacement sound sources.

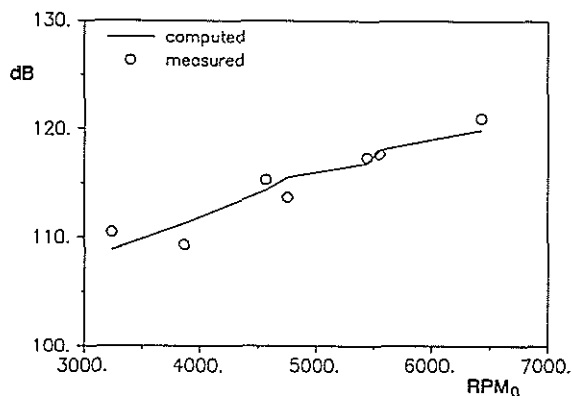


Fig. 20 Inlet SPL for tripped rotor, 1st harmonic, $k = 2$.

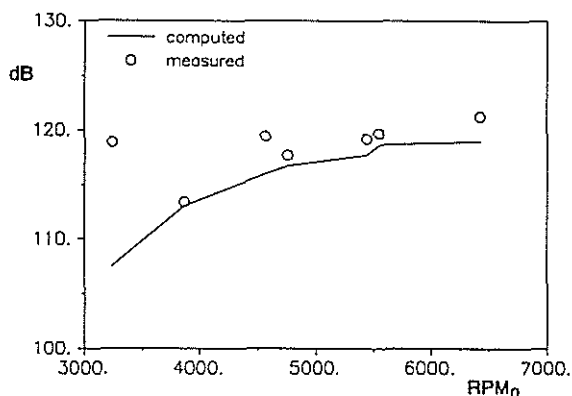


Fig. 21 See Figure 20, for untripped rotor.

In Figures 22 and 23 computed and measured SPL's are plotted for the second harmonic. The extremely low measured results for 4565 RPM₀ fall outside the range of the figures: 83 dB for the tripped rotor and 93 dB for the untripped rotor. The agreement is poor, probably because of inlet reflections.

Finally, it is noted that the first harmonic SPL's with the tripped rotor are lower than with the untripped rotor and, conversely, the second harmonic SPL's with the tripped rotor are higher. This holds for both the theoretical and the measured results and is due to the fact that, in the stator unsteady loading, the contributions of rotor thickness and viscous wakes are in counter-phase in the first harmonic (Figs. 5, 8) and in phase in the second harmonic (Fig. 6).

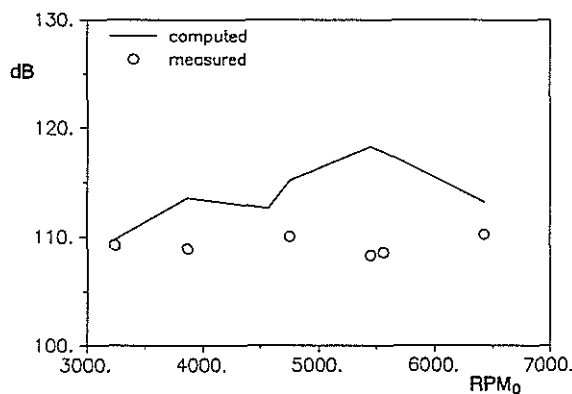


Fig. 22 Inlet SPL for tripped rotor, 2nd harmonic, $k = 4$.

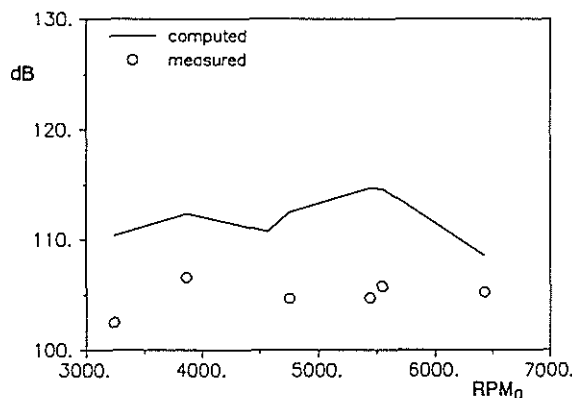


Fig. 23 See Figure 22, for untripped rotor.

VI. Conclusions

A wind tunnel experiment has been carried out with a fan model, designed to study rotor-stator interaction noise. Since the Reynolds numbers were lower than for a typical turbofan stage, trip wires were attached to rotor blades and stator vanes, in order to fix the point of transition from laminar to turbulent boundary flow. The aim of the experiment was the validation of a lifting surface theory for a rotating blade row.

For a range of RPM's the unsteady loading was measured on a rotor blade and the first and the second harmonic were compared with theoretical results. For cases where weak inlet reflections are expected the agreement is good.

Furthermore, inlet wall pressure measurements were compared with results from the theory. For the first harmonic the agreement is good. Small differences, at lower RPM's, can be explained by inlet reflections. For conditions where the inlet reflection is expected to be weak, theoretical and experimental results are within 1 dB! For the second harmonic, however, the agreement is poor, most probably due to reflections.

For a more comprehensive validation, it seems necessary to include acoustic inlet and outlet reflections in the theoretical modelling. In addition, it is advisable to use an experimental model with higher Reynolds numbers, a larger separation of rotor and stator and thinner airfoils.

References

- ¹Tyler, J.M., and Sofrin, T.G., "Axial Flow Compressor Noise Studies", SAE Transactions, Vol. 70, 1962, pp. 309-332.
- ²Schulten, J.B.H.M., *Sound Generation by Ducted Fans and Propellers as a Lifting Surface Problem*, Thesis University of Twente, 1993.
- ³Schulten, J.B.H.M., "Transmission of Sound Through a Rotor", DGLR/AIAA Paper 92-02-085, May 1992.
- ⁴Zandbergen, T., "Stator Vane Response due to the Impingement of the Wake of an Unloaded Rotor", AIAA Paper 88-2814, July 1988.
- ⁵Zandbergen, T., "Experimental Investigation of Rotor Wake-Stator Interaction Noise Generation by Acoustic Mode Measurements", AIAA Paper 89-1126, April 1989.
- ⁶Schulten, J.B.H.M., "Experimental Validation of a Lifting Surface Model for Rotor Wake-Stator Interaction", AIAA Paper 89-1125, April 1989.
- ⁷Schlichting, H., *Boundary Layer Theory*, McGraw-Hill, 1979.
- ⁸Schulten, J.B.H.M., "Vane Sweep Effect on Rotor/Stator Interaction Noise", AIAA Paper 96-1694, May 1996.
- ⁹Abbot, I.H., and Doenhoff, A.E. von, *Theory of Wing Sections*, Dover Publ., 1959.
- ¹⁰Batchelor, G.K., *An Introduction to Fluid Dynamics*, Cambridge University Press, 1967.
- ¹¹Rienstra, S.W., "Acoustic Radiation from a Semi-infinite Annular Duct in a Uniform Subsonic Mean Flow", *Journal of Sound and Vibration*, Vol. 94, No. 2, 1984, pp. 267-288.